Journal of Computational Electronics (2025) 24:104
https://doi.org/10.1007/s10825-025-02348-9

2D material-based plasmonic phototransistors under strong optical excitations

Raonaqul Islam[1] · Ishraq Md. Anjum[1] · Curtis R. Menyuk[1] · Ergun Simsek[1]

Received: 14 December 2024 / Accepted: 14 May 2025

Abstract
Periodic arrays of metallic structures are commonly placed on top of two-dimensional (2D) materials to enhance the local electric field and light absorption, particularly for light detection and generation. However, such enhancement often leads to substantial increases in local temperature under high-power optical excitations. This study explores the feasibility of devising a novel phototransistor with moderate field enhancement yet superior thermal management. Our approach involves strategically placing metal nanoparticles beneath the 2D material and atop silicon pillars. Heat is efficiently transferred to the substrate, mitigating thermal accumulation by leveraging the high thermal conductivity of both metals and silicon. Through multi-physics numerical modeling, our analysis reveals that the proposed design has higher quantum efficiency under high-power excitations than plain and plasmonic phototransistors decorated with metal nanoparticles atop.

Keywords 2D materials · Phototransistors · Quantum efficiency · Thermal management

1 Introduction

Over the past two decades, interest in two-dimensional (2D) materials has grown exponentially due to their unique electrical, optical, and mechanical properties [1–3], rendering them suitable candidates for a variety of photonic and optoelectronic applications [4–16]. A specific group of materials known as transition metal dichalcogenides (TMDs) has emerged as the preferred choice for photosensitive applications, primarily due to their bandgaps falling within the visible to near-infrared portion of the electromagnetic spectrum [3–6, 10–13, 15, 17, 18]. Experimental techniques have been developed to efficiently fabricate these atomically thin structures on silicon, metallic, and glass substrates [19–21]. Notably, TMDs exhibit a direct bandgap when obtained in monolayer forms. While this direct bandgap nature enables moderate photodetection by facilitating a higher generation of electron–hole pairs, it compromises their optical absorption characteristics compared to their bulk counterparts.

Researchers have been exploring different ways of enhancing the absorption of light by these atom-thick materials, for example, by creating Van der Waals heterostructures [22], playing with their chemical formulations [23], and placing plasmonic resonators [10, 11, 14, 17, 24–26] in the vicinity of these 2D materials similar to the plasmonic solar cells [27–30]. For example, Yu *et al.* introduced a method to enhance photocurrent generation in vertical heterostructures of layered materials such as graphene and MoS_2 [22]. Lin *et al.* demonstrated plasmonic enhancement of photocurrent in MoS_2 field-effect transistors decorated with gold nanoparticles [24]. Butun and colleagues demonstrated enhanced light emission from monolayer MoS_2 using plasmonic silver nanodisk arrays, resulting in up to a 12-fold increase in photoluminescence [17]. Bang *et al.* achieved a high-gain MoS_2 photodetector by utilizing the surface plasmon of an Ag nanowire network [25]. Wu *et al.* designed a "gap-mode" plasmon-enhanced monolayer MoS_2 fluorescent emitter and photodetector, overcoming the limited light absorption of 2D materials and achieving significant enhancements in

✉ Ergun Simsek
simsek@umbc.edu

Raonaqul Islam
raonaqi1@umbc.edu

Ishraq Md. Anjum
ianjum1@umbc.edu

Curtis R. Menyuk
menyuk@umbc.edu

[1] Computer Science and Electrical Engineering, University of Maryland Baltimore County, 1000 Hilltop Circle, Baltimore, MD 21250, USA

Published online: 04 June 2025

photoluminescence intensity and photocurrent [26]. Lan *et al.* demonstrated gate-tunable plasmonic phototransistors integrated with monolayer MoS_2, achieving ultrahigh photoresponsivity and a significant enhancement in photocurrent compared to pristine devices [14]. Recently, Koepfli *et al.* experimentally verified 500-gigahertz bandwidth in a graphene-based photodetector, in which they incorporated a metamaterial to enhance the light absorption and engineered the contact design to maximize carrier extraction [16].

In these studies, the researchers generally support their experimental findings with some numerical results generated using the finite-difference time-domain (FDTD) method [10, 14, 16, 17, 26, 31] or the coupled-dipole approximation [32, 33] assuming a constant room temperature of operation. However, in regular plasmonic phototransistors, where metal nanoparticle arrays are fabricated over 2D materials, the temperature inside the 2D material might change dramatically with increasing optical power, leading to a significant drop in the quantum efficiency of the device. In extreme excitation cases, the heat can also cause permanent damage to the device [34].

We previously developed a drift-diffusion model and validated it against experimental results to conduct detailed analyses of two-dimensional (2D) material-based phototransistors [35]. This model assumed a constant operating temperature. In this work, we first extend this model to incorporate local temperature changes arising from Joule heating. After validating the accuracy of this extended model against experimental results found in the literature, we numerically investigate the performance of 2D material-based phototransistors decorated with metal nanoparticles. Our results demonstrate that enhancing the local electric field through plasmonic resonances under weak optical excitations leads to increased quantum efficiency. However, as the optical power increases, this field enhancement causes a significant rise in local temperature, ultimately resulting in a substantial drop in the phototransistor's quantum efficiency. To mitigate this issue and provide a more efficient heat dissipation mechanism, we propose an alternative design: placing metal nanoparticles beneath the 2D material and supporting them with silicon nanopillars. The underlying principle is that while the metal nanoparticles continue to enhance the local electric field, the heat generated around them is effectively collected by the silicon nanopillars and transferred to the silicon substrate, preventing excessive temperature rises. For a proof-of-concept demonstration, we selected monolayer molybdenum disulfide (MoS_2) as our material of choice, leveraging our extensive experimental [3, 10, 11, 36] and numerical [3, 35, 37] experience with this material. Our numerical results indicate that the proposed design exhibits weaker heat buildup and, consequently, a less pronounced reduction in quantum efficiency than traditional plasmonic phototransistors. Therefore, it demonstrates a more stable performance profile, making it a more suitable choice for high-power applications.

The outline of this paper is as follows. We begin by describing the details of our temperature-dependent numerical model, which incorporates the drift-diffusion equations with temperature effects and accounts for Joule heating within monolayer MoS_2. We investigate the impact of assuming a constant temperature versus the proposed temperature-dependent model on quantum efficiency. Furthermore, we validate the accuracy of the model by comparing its predictions with experimental data obtained from plain MoS_2 phototransistors. We then explore the role of plasmonic nanoparticles in enhancing the quantum efficiency of 2D material-based phototransistors. Specifically, we examine the performance variations of designs with nanoparticles placed on top and underneath the MoS_2 layer as a function of incident power. After briefly discussing the practical implications of plasmonic nanoparticle integration, we conclude by summarizing the key findings.

2 Temperature-dependent numerical model and its validation

Figure 1a, c, and d illustrates the 2D material-based phototransistors investigated in this work. The first design does not have nanoparticles (NPs). Figure 1b depicts the equivalent circuit model of this reference phototransistor. In the second design, NPs are positioned directly on top of the 2D material. In the third design, NPs are placed beneath the 2D material, with a small gap separating the top surface of the NPs from the 2D material. A possible fabrication procedure is illustrated in Fig. 2. The process can begin with resist coating, where a thin layer of resist is applied to the substrate to serve as the patterning medium for electron beam lithography (E-beam lithography). Next, E-beam lithography can be performed to expose specific regions of the resist, modifying its solubility and enabling selective removal during the development process. Development might then be carried out to dissolve the exposed resist regions, revealing the underlying substrate in the desired pattern. Once the pattern is defined, the exposed areas of the underlying layer can be etched away, transferring the resist pattern onto the substrate. Following this, a thin layer of metal can be deposited onto the structured surface to form the plasmonic components of the device. The pattern can then be finalized through a lift-off process, in which the remaining resist is removed, leaving behind well-defined metal structures. An RCA cleaning step might be performed to eliminate any residual contaminants. Subsequent processing can include silicon etching to create silicon nanopillars for a more efficient heat dissipation. Afterward, an oxide layer (SiO_2) can be grown to serve

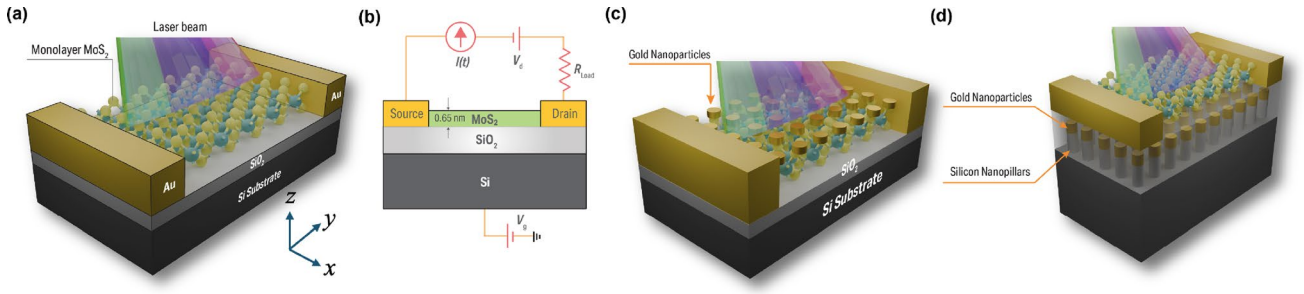

Fig. 1 **a** Schematic view of a plain monolayer MoS_2 phototransistor with metal contacts on both sides and **b** the equivalent circuit model, where V_d and V_g are the applied bias and gate voltages. Schematic views of the plasmonic MoS_2 phototransistors with gold nanoparticles (**c**) on top and (**d**) underneath the MoS_2 layer. For the latter, the nanoparticles are placed on top of silicon nanopillars for more efficient heat dissipation

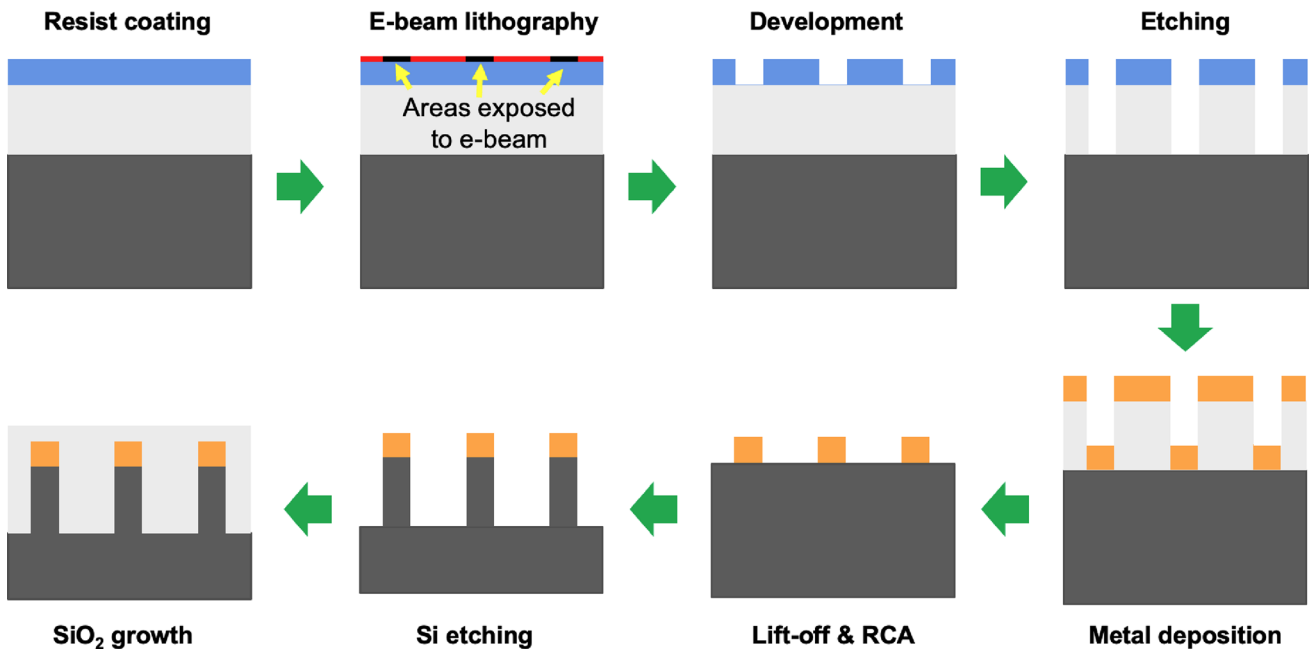

Fig. 2 One possible fabrication process for plasmonic phototransistors with metal nanoparticles positioned beneath the 2D material

as an insulating or protective layer, enhancing device functionality. Once these fabrication steps are complete, MoS_2 can be deposited or transferred using various techniques, either in-house or through a commercial facility, depending on available resources and specific requirements.

For all designs, we assume a monolayer MoS_2 with a thickness of 0.65 nm. Metal contacts are assumed to be made of gold (Au). The SiO_2 layer thickness is 94 nm for the reference design (used for model validation) and 270 nm for the plasmonic phototransistors. Both thicknesses are suitable for providing high contrast between the 2D material-covered and bare substrates [37]. The substrate is silicon (Si) with a 2 μm thickness. V_d and V_g represent the bias (drain-to-source) and back-gate voltages. The phototransistor is illuminated normally from above with an incident electric field given by $E_{inc} = \hat{\mathbf{y}} E_0 e^{-jkz}$, where E_0 is the electric field intensity, $k = 2\pi/\lambda$, and λ is the wavelength of the optical excitation. To analyze the performance of these phototransistors, we adopt the one-dimensional drift-diffusion model proposed in [35]. The model is built on the current continuity equations and the Poisson equation [27, 38]:

$$\begin{aligned} \frac{\delta(n - N_D^+)}{\delta t} &= \frac{\nabla \cdot \mathbf{J}_n}{q} + G - R(n,p), \\ \frac{\delta(p - N_A^-)}{\delta t} &= -\frac{\nabla \cdot \mathbf{J}_p}{q} + G - R(n,p), \\ \nabla \cdot \mathbf{E} &= \frac{q}{\varepsilon}(n - p + N_A^- - N_D^+), \end{aligned} \tag{1}$$

where n is the electron density, p is the hole density, t is time, q is electron's charge, G is generation rate, R is recombination rate, ε is the permittivity of MoS_2, and N_D^+ and N_A^- are the ionized donor and acceptor densities. $\mathbf{J}_n$ and $\mathbf{J}_p$ are electron and hole current densities, respectively, determined by drift-diffusion equations,

$$\begin{aligned}\mathbf{J}_n &= qn\mathbf{v}_n(\mathbf{E}) + qD_n\nabla n\\ \mathbf{J}_p &= qp\mathbf{v}_p(\mathbf{E}) - qD_p\nabla p\end{aligned} \tag{2}$$

where $D_n = k_B T\mu_n/q$ and $D_p = k_B T\mu_p/q$ are the diffusion coefficients of electron and hole, respectively. k_B is the Boltzmann constant, and T is the temperature. μ_n and μ_p are electron and hole mobilities computed with $\mu_{n,p} = 2q\hbar^3 C_s/3k_B T m_{n,p}^2 E_{1n,1p}^2$, where C_s is the stretching modulus, and E_{1n} and E_{1p} are the deformation potential for electrons and holes [39]. $\mathbf{v}_n(\mathbf{E})$ and $\mathbf{v}_p(\mathbf{E})$ are electron and hole drift velocities, respectively, which are evaluated using the famous Caughey–Thomas model [2], $v_{n,p} = \mu_0|\mathbf{E}|/(1+\mu_0|\mathbf{E}|/v_{n,p,sat})$, where μ_0 is the low-field mobility and $|\mathbf{E}|$ is the magnitude of electric field, which can be computed with numerically, for example, using the transfer-matrix method [37] for plain phototransistors and with a finite elements or finite-differences-based numerical solver as it is done in this work.

The G term in Eq. (1) is the electron–hole generation rate of monolayer MoS_2 and determined using the expression: $G = P_0\alpha/AE_{ph}$, where P_0 is the factor corresponding to the incident laser power, α is the absorption coefficient of MoS_2 that is derived from the complex electrical permittivity [3], A is the surface area illuminated by the laser, and E_{ph} is photon's energy. Actual incident power in watts can be calculated by using $P = E_{ph} \times N_P/A$, where N_P is the total number of incident photons during the excitation, which is obtained by integrating the generation rate over the excitation time.

The $R(n, p)$ term in Eq. (1) is the overall recombination rate, which includes the Shockley–Read–Hall recombination, Auger recombination, and radiative recombination [40]. We calculate the total recombination using the following formula:

$$R(n,p) = (np - n_i^2)\times \left[\frac{1}{(n+n_i)\tau_p + (p+n_i)\tau_n} + C_n n + C_p p + B_r\right] \tag{3}$$

where n_i is the intrinsic carrier concentration, τ_p and τ_n are hole and electron lifetimes, respectively, C_n and C_p are the Auger recombination rates of electrons and holes respectively, and B_r is the radiative recombination rate. To account for the applied gate voltage, we assume the MoS_2 monolayer is intrinsically n-doped due to surface traps with a doping density of N_{traps}. When the gate voltage (V_g) exceeds a threshold value (V_{th}), the doping density is determined using the expression $n_s = \varepsilon_{ox}(V_g - V_{th})/t_{ox}$, where the threshold voltage is given by $V_{th} = N_{traps}t_{ox}/\varepsilon_{ox}$. Here, t_{ox} represents the oxide layer thickness, and ε_{ox} is the permittivity of the oxide layer.

We adopt the simple temperature model discussed in [41] to evaluate the temperature increase inside the MoS_2 film due to Joule heating. Under steady-state condition, the temperature change because of Joule heating can be computed with $-\nabla\cdot\sigma_T\nabla T = \mathbf{J}\cdot\mathbf{E}$. We can deduce an approximation from this equation to estimate the temperature increase inside the MoS_2 layer with the following expression,

$$\nabla T \approx |\mathbf{J}\cdot\mathbf{E}|/\sigma_T L \tag{4}$$

where $\mathbf{J} = \mathbf{J}_n + \mathbf{J}_p$ is the total current density, L is the length of the phototransistor, and σ_T is the thermal conductivity of monolayer MoS_2, which is approximated by using a simple model, $\sigma_T(T) = 1370e^{-0.0315T} + 156e^{-0.0048T}$. This formula provides a good approximation of the thermal conductivity for monolayer MoS_2 determined with first principle calculations [42]. The rest of the material parameters are summarized in Table 1. Refractive indices of the other materials used in this work, which are Si, SiO_2, and Au, can be found in [43, 44], and [45], respectively.

Before evaluating its accuracy, we first investigate the expected discrepancy between this temperature-dependent model and our previous model [35], which assumed a constant operating temperature. A 1 μm by 1 μm monolayer MoS_2 is placed on a 94-nm-thick SiO_2 layer atop a Si substrate. We assume a trap density, $N_{traps} = 10^{10}$ cm^{-2}, for all cases presented here. Figure 3a illustrates the reflectance from this structure as a function of incident wavelength and the intensity of the electric field at the center of the MoS_2 film. Consistent with experimental findings [3], the reflectance is strong at shorter wavelengths, diminishes with increasing λ, and exhibits oscillations around the red region of the spectrum. Notably, the peak in electric field intensity occurs at a wavelength distinct from the wavelength of minimum reflectance. This behavior is attributed to the refractive indices and thicknesses of the substrate layers, as detailed in [35]. Figure 3b presents the quantum efficiency of this phototransistor for $\lambda = 575$ nm, $V_d = 0.5$ V, and $V_g = 10$ V. The solid and dashed curves represent the numerical results obtained using our previous fixed-temperature model [35] (assuming $T = 300$ K) and the proposed temperature-dependent model, respectively, where the local temperature is calculated using Eq. (4). As expected, the models exhibit negligible differences at very low optical powers. However, the new temperature-dependent model predicts a more significant decrease in quantum efficiency with increasing incident power.

To validate the accuracy of this temperature-dependent numerical model, we compare its predictions to experimental measurements on a bare MoS_2 phototransistor

Table 1 Material parameters of MoS_2 used in our calculations. m_0 is the electron mass

Parameter name	Symbol	Value
Energy bandgap [46]	E_g	$1.95 - 5.9 \times 10^{-4} T^2/(T + 430)$ eV
Electron's effective mass [47]	m_n	$0.35 m_0$
Hole's effective mass [47]	m_p	$0.50 m_0$
Electron affinity [7]	χ_i	4.27 eV
Radiative recombination coefficient [8]	B_r	$10^{-7}\ cm^3/s$
Auger coefficient [8]	C_n, C_p	$10^{-24}\ cm^6/s$
Density of states in conduction band [48]	N_C	$3.76 \times 10^{11}\ cm^{-2}$
Density of states in valence band [48]	N_V	$5.76 \times 10^{11}\ cm^{-2}$
Hole saturation velocity [49]	$v_{p,sat}$	$1 \times 10^7\ cm/s$
Electron saturation velocity [49]	$v_{n,sat}$	$4.2 \times 10^6\ cm/s$
Electron lifetime [9]	τ_n	$1 \times 10^{-9}\ s$
Stretching modulus [39]	C_s	138.2 N/m
Deformation potential for electrons [39]	E_{1n}	11.02 eV
Deformation potential for holes [39]	E_{1p}	5.05 eV
Hole lifetime [9]	τ_p	$1 \times 10^{-8}\ s$
Mass density [50]	ρ	5060 kg/m^3
Specific heat [51]	c_v	255104 J/kgK
Thermal conductivity [52]	κ	23.2 W/mK

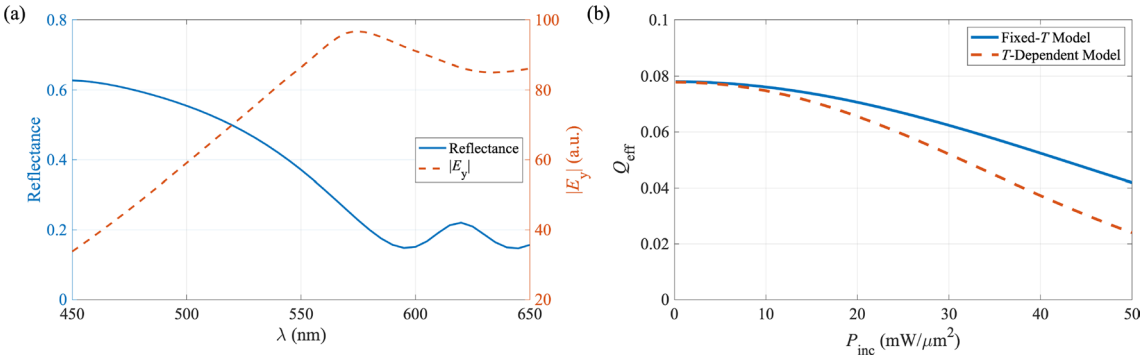

Fig. 3 **a** The blue solid curve is the reflectance from a MoS_2-coated SiO_2/Si substrate as a function of wavelength, and the dashed red curve is the electric field intensity at the center of the MoS_2 film. **b** Quantum efficiency of this phototransistor as a function of incident power calculated assuming a constant temperature of operation (solid curve) and temperature-dependent model (dashed curve)

studied in [12]. The MoS_2 film has dimensions of 5 μm in width and 4 μm in length. First, we set the excitation wavelength to 532 nm and the incident power to 15 mW/μm^2. We then calculate the output current (I_d) as a function of the drain-to-source voltage (V_d) for a gate voltage of $V_g = 25$ V. Figure 4a demonstrates a good agreement between our numerical results and the experimental data presented in [12]. Next, we compute the temperature increase at the center of the MoS_2 film as a function of incident power for $V_d = 4$ V and $V_g = 25$ V. Figure 4b again reveals strong agreement between our numerical results and the experimental findings reported in [12].

3 Excito-plasmonic phototransistors

Next, we examine the performance of the phototransistors depicted in Fig. 1c and d. We refer to these devices as excito-plasmonic phototransistors because they leverage the interaction between excitons (electron–hole pairs within the semiconductor film) and plasmons (collective oscillations of electrons within or on the surface of the metal NPs) to enhance light detection capabilities. This coupled interaction is expected to amplify the photocurrent generated by light exposure [14].

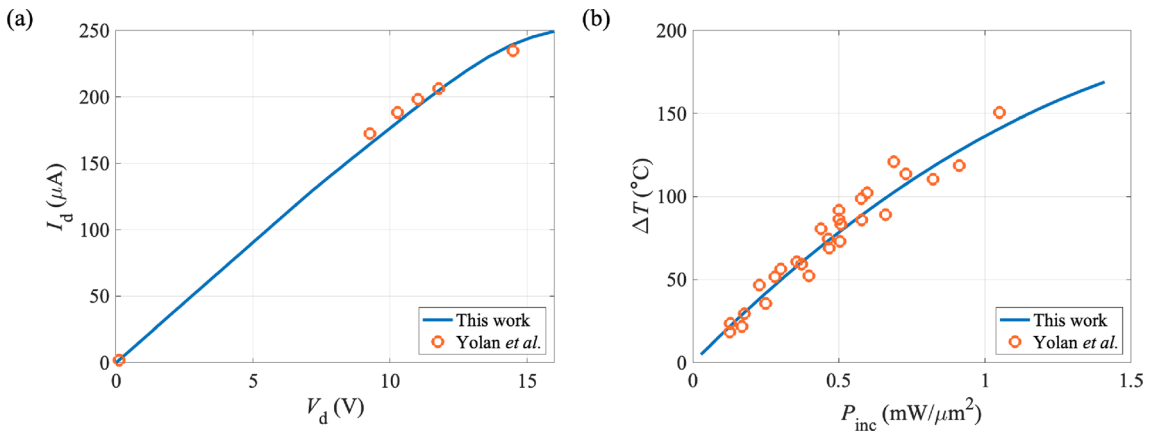

Fig. 4 **a** Output current vs. drain-to-source voltage for a $5\mu m \times 4\mu m$ monolayer MoS_2-coated SiO_2/Si substrate for $V_g = 25$ V, $\lambda = 532$ nm, and $P = 15$ mW/μm^2. **b** Temperature increase inside the monolayer MoS_2 vs. incident power for $V_d = 4$ V, $V_g = 25$ V, and $\lambda = 532$ nm

We first consider a scenario where a gold nanoparticle array is positioned atop a MoS_2 layer, which is itself deposited on a 270-nm-thick SiO_2 layer on a Si substrate, as illustrated in Fig. 1c. The MoS_2 film dimensions are 5 μm by 4 μm, with $V_g = 25V$, and $V_d = 10$ V. The cylindrical Au NPs have a diameter of 75 nm and a height of 65 nm, arranged with an inter-particle spacing of 200 nm in the lateral directions. The blue solid curves in Fig. 5a–c depict the local enhancement ratio for the y-component of the electric field intensity for three distinct excitation wavelengths: 475 nm, 550 nm, and 625 nm, respectively. Here, the local enhancement ratio is defined as the ratio of the y-component of the electric field intensity at the center of the MoS_2 layer (i.e., at $z = 0.325$ nm) with and without the presence of NPs. In all cases, we observe significant field enhancement near the NP edges, highlighted by red-shaded regions. Figure 5d presents

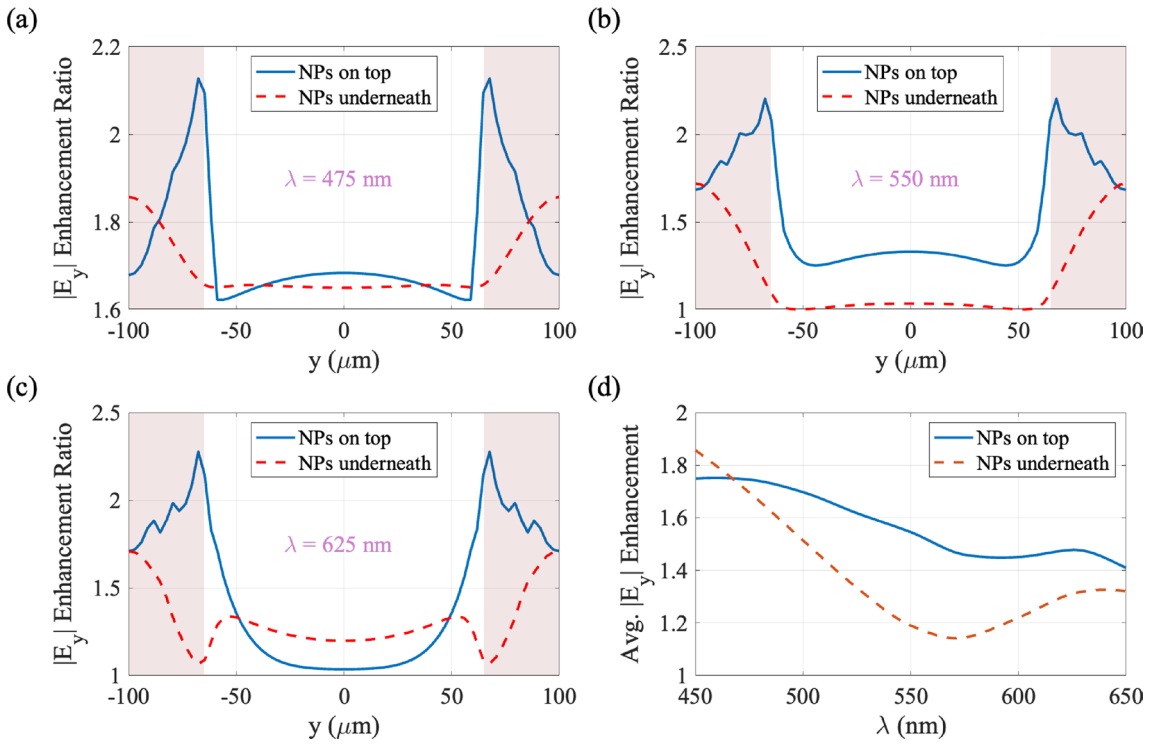

Fig. 5 Electric field intensity inside the monolayer MoS_2 with the nanoparticles on top (solid curves) and underneath (dashed curves) of the MoS_2 layer for (**a**) $\lambda = 475$ nm, (**b**) $\lambda = 550$ nm, and (**c**) $\lambda = 625$ nm. The red-shaded regions correspond to the location of NPs. (**d**) Electric field intensity averaged along the MoS_2 layer as a function of λ

the enhancement ratio averaged across the entire MoS_2 film as a function of the incident wavelength. We then repeat these calculations for the excito-plasmonic phototransistor depicted in Fig. 1d. In this configuration, the metal NPs are positioned beneath the MoS_2 layer and on top of 200 nm tall Si nanopillars with a diameter of 75 nm. Since the SiO_2 layer is 270 nm thick, a 5 nm gap exists between the Au NPs and the bottom surface of the MoS_2 film. This design is motivated by silicon's significantly higher thermal conductivity than SiO_2. We anticipate that the heat generated by the enhanced local electric field can be more effectively transferred to the silicon substrate due to the high thermal conductivity of both gold and silicon. The dashed red curves in Fig. 5 illustrate the local and averaged enhancement ratios for this configuration. Two key observations emerge from Fig. 5a–c as follows. First, the field enhancement is most pronounced directly on top of the Au NPs, rather than near their edges. This suggests that the Au NPs function more like reflectors in this arrangement. Second, the average field enhancement is weaker compared to the design with Au NPs positioned on top of the MoS_2 layer. This is unsurprising, as the Au NPs are not in direct contact with the MoS_2 film in this proposed design. In Fig. 5d, we plot the electric field enhancement ratios averaged along the MoS_2 layer as a function of λ. Based on these average enhancement ratios, we expect a comparable level of improvement in quantum efficiency (relative to the bare phototransistor) at $\lambda = 475$ nm for both designs. At longer wavelengths, the excito-plasmonic phototransistor with NPs positioned on top should exhibit a higher quantum efficiency than the design with NPs positioned underneath, particularly at low excitation powers. At wavelengths close to 450 nm, we observe that the design with NPs underneath has a stronger average field enhancement, despite the results presented in Fig. 5a–c. This observation highlights a fundamental challenge in plasmonic structure design for field enhancement, where the apparent inconsistency stems from competing mechanisms between top and bottom nanoparticle (NP) placement. While NPs on top generate strong near-field enhancement via localized surface plasmon resonance (LSPR) at their edges, they simultaneously act as efficient scatterers, reflecting more incident energy than the bare MoS_2-coated substrate. In contrast, NPs positioned underneath the MoS_2 layer exhibit two counteracting effects: Their LSPR-induced enhancement is weakened due to reduced light coupling and lack of direct contact with MoS_2, yet they simultaneously function as nanoscale mirrors that reflect incident light back into the MoS_2 layer, thereby increasing the local optical density. Notably, at shorter wavelengths below 475 nm (particularly around 450 nm), this interplay leads to marginally stronger average field enhancement for subsurface NPs compared to surface-positioned ones. These competing processes—plasmonic enhancement versus scattering and reflection losses—underscore the delicate balance required when engineering plasmonic-photonic hybrid systems for optimal performance.

The central question we aim to address next is: "How does the quantum efficiency change with increasing optical excitation strength?" However, before we try to answer this question, let us share some numerical results obtained with a commercial software package, Lumerical Heat. We place a heat source λ above the phototransistors and determine the steady-state temperature inside the MoS_2 layer for heat flux values ranging from 0.1 μW to 0.1 mW, corresponding to 50 $\mu W/\mu m^2$ – 50 $mW/\mu m^2$ of incident optical powers. Figure 6a shows the local temperature at the center of the MoS_2 film for the phototransistors with and without NPs. As expected, the plain phototransistor experiences the weakest heating, and the phototransistor with NPs on top experiences the most substantial heating. In all cases, we observe that the induced temperature in monolayer MoS_2 has almost a linear relationship with absorbed power, where the function's slope is approximately equal to the thermal boundary conductance (TBC), $G = 20$ $MWm^{-2}K^{-1}$, similar to the results provided [53]. In Fig. 6 b–d, we plot the temperature distributions over the MoS_2 layer for the plain and plasmonic phototransistors for $P_{inc} = 50$ $mW/\mu m^2$. As expected, under this very strong excitation, the temperature inside the MoS_2 layer reaches around 530 K for the phototransistor with NPs on top. However, for the proposed design, the maximum temperature is around 380 K for the same optical excitation.

Figure 7a–c presents the quantum efficiency (Q_{eff}) of MoS_2 phototransistors as a function of incident power (P_{inc}) for three wavelengths: 475 nm, 550 nm, and 625 nm. The blue dashed, red dotted, and yellow solid curves correspond to the phototransistors without NPs, with NPs on top of the MoS_2 layer, and with NPs underneath it, respectively. For $\lambda = 475$ nm, Fig. 7a, the quantum efficiency decreases with increasing incident power for all configurations. The configuration with NPs on top exhibits the highest Q_{eff} at weak optical excitations, indicating enhanced light absorption due to plasmonic effects. However, this enhancement comes at the cost of increased local heating with increasing incident power, as evidenced by the steep rise in T_{max} in Fig. 6a for this design. When NPs are placed beneath the MoS_2 layer and on top of the silicon pillars, the quantum efficiency is lower but still surpasses that of the configuration without NPs. This configuration facilitates better heat dissipation due to the high thermal conductivity of the underlying silicon pillars, resulting in significantly lower temperatures than the phototransistor with NPs on top. For $\lambda = 550$ nm, shown in Fig. 7b, the trends are similar. While the quantum efficiency improvement due to NPs on top is substantial at low incident power, this configuration suffers from excessive local heating. In fact, its performance deteriorates to below that of

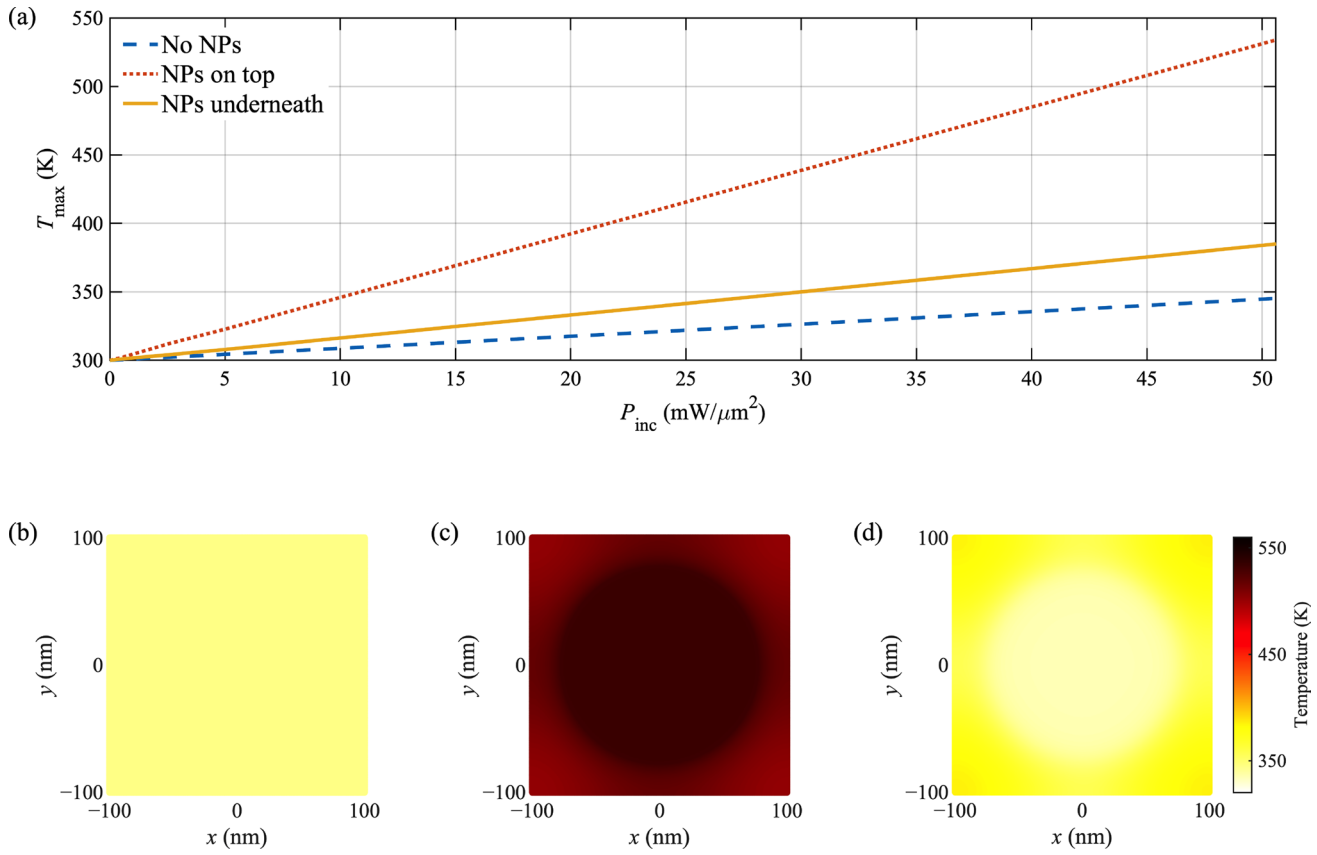

Fig. 6 **a** Maximum temperature as a function of input optical power for the phototransistors without NPs (blue dashed curve), with NPs on top (red dotted curve) and NPs underneath (yellow solid curve). Heat profiles of (**b**) bare MoS_2 transistors and plasmonic phototransistors with NPs (**c**) on top and (**d**) underneath the MoS_2 layer for $P_{inc} = 50$ mW/μm^2

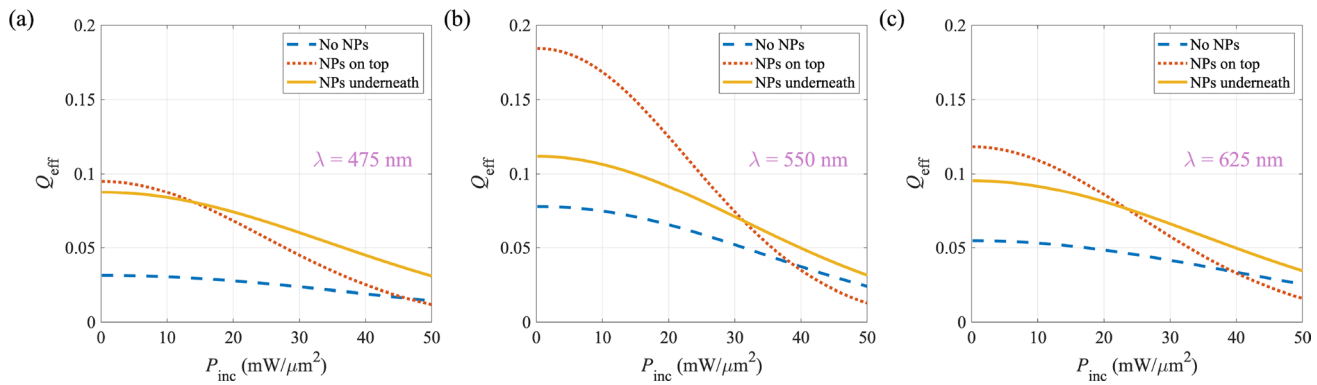

Fig. 7 Quantum efficiency of MoS_2 phototransistors without NPs (dotted curves), NPs on top (dashed curves), and NPs beneath (solid curves) the monolayer MoS_2 layer as a function of incident power for (**a**) $\lambda = 475$ nm, (**b**) $\lambda = 550$ nm, and (**c**) $\lambda = 625$ nm

the plain phototransistor for optical excitations exceeding 38 mW/μm^2. In contrast, the design with NPs underneath maintains a balance between moderate quantum efficiency enhancement and effective heat dissipation. For $\lambda = 625$ nm, Fig. 7c, the quantum efficiency is lower across all configurations compared to that at $\lambda = 550$ nm, reflecting reduced red light absorption by the monolayer MoS_2. The configuration with NPs on top still achieves the highest Q_{eff} under weak optical excitation, but the decline in efficiency with increasing P_{inc} is more pronounced, again due to thermal effects. The configuration with NPs underneath provides a more stable performance, with limited heating

and consistent quantum efficiency enhancement over the nanoparticle-free design.

These results demonstrate that enhancing the local electric field with plasmonic resonances effectively increases light absorption by the 2D material, boosting photocurrent under weak or moderate optical excitations. However, under strong optical excitations, the field enhancement can lead to significant temperature increases, ultimately diminishing the device's efficiency in converting absorbed photons to electrical currents. The low thermal conductivity of SiO_2 hinders efficient heat dissipation. To mitigate this issue, placing metal NPs beneath the 2D material and on top of silicon nanopillars (or employing a thin SiO_2 layer and directly fabricating metal NPs on top of the silicon layer) can provide a more effective heat dissipation mechanism. This approach may result in weaker plasmonic resonances but offers more stable and quantumly efficient performance (compared to designs with NPs on top) across a broader range of optical excitations. This design trade-off underscores the importance of optimizing nanoparticle placement not only for optical performance but also for thermal management. Considering the very low quantum efficiency of 2D material-based photodetectors, even a small improvement in quantum efficiency, from 4% to 6%, is crucial, particularly for applications demanding low phase noise and high bandwidth [35].

Before concluding, we note that this study does not account for the tunneling effect. In the proposed design, where there is no direct physical contact between the nanoparticles and the semiconductor film, the metal nanoparticles influence the system primarily through their electric fields. This effect has already been incorporated into our calculations, which evaluate the local electric field within the semiconductor film. However, if the separation between the nanoparticles and the semiconductor film is sufficiently small, charge carriers from the semiconductor may tunnel into the nanoparticles, potentially enhancing recombination. At this stage, we have not included this tunneling effect in our analysis. Future experimental studies will help determine whether this phenomenon warrants further consideration.

4 Conclusion

In summary, we have developed a temperature-dependent drift-diffusion model to accurately predict the performance of 2D material-based phototransistors under varying-power optical excitations. Our model accounts for Joule heating and its impact on device characteristics. We then investigated the performance of plasmonic phototransistors, where metal nanoparticles are strategically placed to enhance light absorption. While these structures demonstrate significant quantum efficiency improvements under weak optical excitations, they suffer from substantial temperature increases due to Joule heating, leading to a decline in performance at higher powers. To address this, we propose a novel design where metal nanoparticles are placed beneath the 2D material and supported by silicon nanopillars. This configuration enables more efficient heat dissipation, leading to more stable and consistent quantum efficiency enhancement across a wider range of optical powers. Our findings highlight the critical importance of considering thermal management alongside optical field enhancement in the design of high-performance 2D material-based photodetectors for demanding applications.

Author contributions E.S. wrote the initial code. I.A. and R.I. improved the code to be able to work with 2D materials. R.I. and E.S. wrote the main manuscript. All authors reviewed the manuscript.

Funding This work was supported by internal funding from the College of Engineering and Information Technology (COEIT) at the University of Maryland Baltimore County (UMBC) through the Interdisciplinary Research Programs (IRP) initiative.

Data availability statement Data that support the findings of this study and MATLAB codes to produce the presented figures can be found at https://github.com/simsekergun/EPP

Declarations

Conflict of interest The authors declare no conflict of interest.

References

1. Pak, J., Lee, I., Cho, K., Kim, J.-K., Jeong, H., Hwang, W.-T., Ahn, G.H., Kang, K., Yu, W.J., Javey, A., Chung, S., Lee, T.: Intrinsic optoelectronic characteristics of MoS_2 phototransistors via a fully transparent Van der Waals heterostructure. ACS Nano **13**(8), 9638–9646 (2019). https://doi.org/10.1021/acsnano.9b04829. (**PMID: 31345021**)
2. Smithe, K.H. Kirby., English, C.D., Suryavanshi, S.V., Pop, E.: High-field transport and velocity saturation in synthetic monolayer MoS_2. Nano Lett. **18**(7), 4516–4522 (2018). https://doi.org/10.1021/acs.nanolett.8b01692. (**PMID: 29927605**)
3. Mukherjee, B., Tseng, F., Gunlycke, D., Amara, K.K., Eda, G., Simsek, E.: Complex electrical permittivity of the monolayer molybdenum disulfide (MoS_2) in near UV and visible. Opt. Mater. Expr. **5**(2), 447–455 (2015). https://doi.org/10.1364/OME.5.000447

4. Mak, K.F., Lee, C., Hone, J., Shan, J., Heinz, T.F.: Atomically thin MoS_2: A new direct-gap semiconductor. Phys. Rev. Lett. **105**, 136805 (2010). https://doi.org/10.1103/PhysRevLett.105.136805
5. Yin, Z., Li, H., Li, H., Jiang, L., Shi, Y., Sun, Y., Lu, G., Zhang, Q., Chen, X., Zhang, H.: Single-layer MoS_2 phototransistors. ACS Nano **6**(1), 74–80 (2012). https://doi.org/10.1021/nn2024557. (**PMID: 22165908**)
6. Mak, K.F., He, K., Lee, C., Lee, G.H., Hone, J., Heinz, T.F., Shan, J.: Tightly bound trions in monolayer MoS_2. Nature Mater. **12**, 207–211 (2013)
7. Gong, C., Zhang, H., Wang, W., Colombo, L., Wallace, R.M., Cho, K.: Band alignment of two-dimensional transition metal dichalcogenides: Application in tunnel field effect transistors. Appl. Phys. Lett. **103**(5), 053513 (2013). https://doi.org/10.1063/1.4817409
8. Salehzadeh, O., Tran, N.H., Liu, X., Shih, I., Mi, Z.: Exciton kinetics, quantum efficiency, and efficiency droop of monolayer MoS_2 light-emitting devices. Nano Lett. **14**(7), 4125–4130 (2014). https://doi.org/10.1021/nl5017283. (**PMID: 24905765**)
9. Chen, W., Yin, W.-Y., Zhao, W.-S., Hao, R., Li, E., Kang, K., Guo, J.: Scaling analysis of high gain monolayer MoS_2 photodetector for its performance optimization. IEEE Trans. Electron Devices **63**(4), 1608–1614 (2016). https://doi.org/10.1109/TED.2016.2532908
10. Mukherjee, B., Simsek, E.: Plasmonics enhanced average broadband absorption of monolayer MoS_2. Plasmonics **11**(1), 285–289 (2016). https://doi.org/10.1007/s11468-015-0053-9
11. Mukherjee, B., Leong, W.S., Li, Y., Gong, H., Sun, L., Shen, Z.X., Simsek, E., Thong, J.T.L.: Raman analysis of gold on WSe_2 single crystal film. Mater. Res. Expr. **2**(6), 065009 (2015). https://doi.org/10.1088/2053-1591/2/6/065009
12. Yalon, E., McClellan, C.J., Smithe, K.K.H., Muñoz Rojo, M., Xu, R.L., Suryavanshi, S.V., Gabourie, A.J., Neumann, C.M., Xiong, F., Farimani, A.B., Pop, E.: Energy dissipation in monolayer MoS_2 electronics. Nano Lett. **17**(6), 3429–3433 (2017). https://doi.org/10.1021/acs.nanolett.7b00252
13. Vaquero, D., Clericò, V., Salvador-Sánchez, J., Díaz, E., Domínguez-Adame, F., Chico, L., Meziani, Y.M., Diez, E., Quereda, J.: Fast response photogating in monolayer MoS_2 phototransistors. Nanoscale **13**, 16156–16163 (2021). https://doi.org/10.1039/D1NR03896F
14. Lan, H.-Y., Hsieh, Y.-H., Chiao, Z.-Y., Jariwala, D., Shih, M.-H., Yen, T.-J., Hess, O., Lu, Y.-J.: Gate-tunable plasmon-enhanced photodetection in a monolayer MoS_2 phototransistor with ultrahigh photoresponsivity. Nano Lett. **21**(7), 3083–3091 (2021). https://doi.org/10.1021/acs.nanolett.1c00271
15. Li, Y., Li, L., Li, S., Sun, J., Fang, Y., Deng, T.: Highly sensitive photodetectors based on monolayer MoS_2 field-effect transistors. ACS Omega **7**(16), 13615–13621 (2022). https://doi.org/10.1021/acsomega.1c07117
16. Koepfli, S.M., Baumann, M., Koyaz, Y., Gadola, R., Güngör, A., Keller, K., Horst, Y., Nashashibi, S., Schwanninger, R., Doderer, M., et al.: Metamaterial graphene photodetector with bandwidth exceeding 500 gigahertz. Science **380**(6650), 1169–1174 (2023)
17. Butun, S., Tongay, S., Aydin, K.: Enhanced light emission from large-area monolayer MoS_2 using plasmonic nanodisc arrays. Nano Lett. **15**(4), 2700–2704 (2015). https://doi.org/10.1021/acs.nanolett.5b00407
18. Lv, R., Robinson, J.A., Schaak, R.E., Sun, D., Sun, Y., Mallouk, T.E., Terrones, M.: Transition metal dichalcogenides and beyond: Synthesis, properties, and applications of single- and few-layer nanosheets. Accounts Chem. Res. **48**, 56–64 (2015). https://doi.org/10.1021/ar5002846
19. Coleman, J.N., Lotya, M., O'Neill, A., Bergin, S.D., King, P.J., Khan, U., Young, K., Gaucher, A., De, S., Smith, R.J., Shvets, I.V., Arora, S.K., Stanton, G., Kim, H.-Y., Lee, K., Kim, G.T., Duesberg, G.S., Hallam, T., Boland, J.J., Wang, J.J., Donegan, J.F., Grunlan, J.C., Moriarty, G., Shmeliov, A., Nicholls, R.J., Perkins, J.M., Grieveson, E.M., Theuwissen, K., McComb, D.W., Nellist, P.D., Nicolosi, V.: Two-dimensional nanosheets produced by liquid exfoliation of layered materials. Science **331**(6017), 568–571 (2011). https://doi.org/10.1126/science.1194975
20. Castellanos-Gomez, A., Barkelid, M., Goossens, A.M., Calado, V.E., Zant, H.S.J., Steele, G.A.: Laser-thinning of MoS_2: On demand generation of a single-layer semiconductor. Nano Lett. **12**(6), 3187–3192 (2012). https://doi.org/10.1021/nl301164v. (**PMID: 22642212**)
21. Mannix, A.J., Kiraly, B., Hersam, M.C., Guisinger, N.P.: Synthesis and chemistry of elemental 2D materials. Nature Rev. Chem. **1**(2), 0014 (2017). https://doi.org/10.1038/s41570-016-0014
22. Yu, W.J., Liu, Y., Zhou, H., Yin, A., Li, Z., Huang, Y., Duan, X.: Highly efficient gate-tunable photocurrent generation in vertical heterostructures of layered materials. Nature Nanotechnol. **8**(12), 952–958 (2013). https://doi.org/10.1038/nnano.2013.219
23. Amani, M., Lien, D.-H., Kiriya, D., Xiao, J., Azcatl, A., Noh, J., Madhvapathy, S.R., Addou, R., Kc, S., Dubey, M., Cho, K., Wallace, R.M., Lee, S.-C., He, J.-H., Ager, J.W., Zhang, X., Yablonovitch, E., Javey, A.: Near-unity photoluminescence quantum yield in MoS_2. Science **350**(6264), 1065–1068 (2015). https://doi.org/10.1126/science.aad2114
24. Lin, J., Li, H., Zhang, H., Chen, W.: Plasmonic enhancement of photocurrent in MoS_2 field-effect-transistor. Appl. Phys. Lett. **102**(20), 203109 (2013). https://doi.org/10.1063/1.4807658
25. Bang, S., Duong, N.T., Lee, J., Cho, Y.H., Oh, H.M., Kim, H., Yun, S.J., Park, C., Kwon, M.-K., Kim, J.-Y., Kim, J., Jeong, M.S.: Augmented quantum yield of a 2D monolayer photodetector by surface plasmon coupling. Nano Lett. **18**(4), 2316–2323 (2018). https://doi.org/10.1021/acs.nanolett.7b05060
26. Wu, Z.-Q., Yang, J.-L., Manjunath, N.K., Zhang, Y.-J., Feng, S.-R., Lu, Y.-H., Wu, J.-H., Zhao, W.-W., Qiu, C.-Y., Li, J.-F., Lin, S.-S.: Gap-mode surface-plasmon-enhanced photoluminescence and photoresponse of MoS_2. Adv. Mater. **30**(27), 1706527 (2018). https://doi.org/10.1002/adma.201706527
27. Li, X., Hylton, N.P., Giannini, V., Lee, K.-H., Ekins-Daukes, N.J., Maier, S.A.: Multi-dimensional modeling of solar cells with electromagnetic and carrier transport calculations. Progress in Photovoltaics: Res. Appl. **21**(1), 109–120 (2013). https://doi.org/10.1002/pip.2159
28. An, Y., Sheng, C., Li, X.: Radiative cooling of solar cells: Opto-electro-thermal physics and modeling. Nanoscale **11**(36), 17073–17083 (2019). https://doi.org/10.1039/C9NR04110A
29. Saxena, P., Gorji, N.E.: Comsol simulation of heat distribution in perovskite solar cells: coupled optical-electrical-thermal 3-D analysis. IEEE J. Photovoltaics **9**(6), 1693–1698 (2019). https://doi.org/10.1109/JPHOTOV.2019.2940886
30. Hylton, N., Li, X., Giannini, V., Lee, K.-H., Ekins-Daukes, N., Loo, J., Vercruysse, D., Van Dorpe, P., Sodabanlu, H., Sugiyama, M., et al.: Loss mitigation in plasmonic solar cells: aluminium nanoparticles for broadband photocurrent enhancements in GaAs photodiodes. Sci. Rep. **3**(1), 2874 (2013). https://doi.org/10.1038/srep02874
31. Zhou, W., Odom, T.W.: Tunable subradiant lattice plasmons by out-of-plane dipolar interactions. Nature Nanotechnol. **6**(7), 423–427 (2011). https://doi.org/10.1038/nnano.2011.72
32. Kravets, V.G., Kabashin, A.V., Barnes, W.L., Grigorenko, A.N.: Plasmonic surface lattice resonances: A review of properties and applications. Chem. Rev. **118**(12), 5912–5951 (2018). https://doi.org/10.1021/acs.chemrev.8b00243
33. Simsek, E.: Improving tuning range and sensitivity of localized SPR sensors with graphene. IEEE Photonics Technol.

Lett. **25**(9), 867–870 (2013). https://doi.org/10.1109/LPT.2013.2253316
34. Yeshchenko, O.A., Dmitruk, I.M., Alexeenko, A.A., Kotko, A.V., Verdal, J., Pinchuk, A.O.: Size and temperature effects on the surface plasmon resonance in silver nanoparticles. Plasmonics **7**, 685–694 (2012). https://doi.org/10.1007/s11468-012-9359-z
35. Islam, R., Anjum, I.M., Menyuk, C.R., Simsek, E.: Study of an MoS_2 phototransistor using a compact numerical method enabling detailed analysis of 2d material phototransistors. Sci. Rep. **14**(1), 15269 (2024). https://doi.org/10.1038/s41598-024-66171-1
36. Mukherjee, B., Guchhait, A., Chan, Y., Simsek, E.: Absorptance of PbS quantum dots thin film deposited on trilayer MoS_2. Adv. Mater. Lett. **6**(11), 936–940 (2015)
37. Simsek, E., Mukherjee, B.: Visibility of atomically-thin layered materials buried in silicon dioxide. Nanotechnology **26**(45), 455701 (2015). https://doi.org/10.1088/0957-4484/26/45/455701
38. Wilson, S.P., Walker, A.B.: One- and two-dimensional models of the transient response of metal - semiconductor - metal photodetectors including diffraction. Semiconductor Sci. Technol. **12**, 1265–1272 (1999)
39. Phuc, H.V., Hieu, N.N., Hoi, B.D., Hieu, N.V., Thu, T.V., Hung, N.M., Ilyasov, V.V., Poklonski, N.A., Nguyen, C.V.: Tuning the electronic properties, effective mass and carrier mobility of MoS_2 monolayer by strain engineering: First-principle calculations. J. Electron. Mater. **47**(1), 730–736 (2018). https://doi.org/10.1007/s11664-017-5843-8
40. Razeghi, M.: In: Razeghi, M. (ed.) Non-equilibrium Electrical Properties of Semiconductors, pp. 275–318. Springer, Cham (2019). https://doi.org/10.1007/978-3-319-75708-7
41. Simsek, E., Hastings, A.S., Tulchinsky, D.A., Williams, K.J., Menyuk, C.R.: A simple numerical model to estimate the temperature distributions over photodetectors in steady-state. IEEE Photonics J. **16**(3), 1–6 (2024). https://doi.org/10.1109/JPHOT.2024.3397857
42. Yan, R., Simpson, J.R., Bertolazzi, S., Brivio, J., Watson, M., Wu, X., Kis, A., Luo, T., Hight Walker, A.R., Xing, H.G.: Thermal conductivity of monolayer molybdenum disulfide obtained from temperature-dependent Raman spectroscopy. ACS Nano **8**(1), 986–993 (2014). https://doi.org/10.1021/nn405826k. (**PMID: 24377295**)
43. Green, M.A.: Self-consistent optical parameters of intrinsic silicon at 300k including temperature coefficients. Solar Energy Mater. Solar Cells **92**(11), 1305–1310 (2008). https://doi.org/10.1016/j.solmat.2008.06.009
44. Malitson, I.H.: Interspecimen comparison of the refractive index of fused silica. J. Optical Soc. Am. **55**(10), 1205–1209 (1965). https://doi.org/10.1364/JOSA.55.001205
45. Rakić, A.D., Djurišić, A.B., Elazar, J.M., Majewski, M.L.: Optical properties of metallic films for vertical-cavity optoelectronic devices. Appl. Optics **37**(22), 5271–5283 (1998). https://doi.org/10.1364/AO.37.005271
46. Korn, T., Heydrich, S., Hirmer, M., Schmutzler, J., Schüller, C.: Low-temperature photocarrier dynamics in monolayer MoS_2. Appl. Phys. Lett. **99**(10), 102109 (2011). https://doi.org/10.1063/1.3636402
47. Cheiwchanchamnangij, T., Lambrecht, W.R.L.: Quasiparticle band structure calculation of monolayer, bilayer, and bulk MoS_2. Phys. Rev. B **85**, 205302 (2012). https://doi.org/10.1103/PhysRevB.85.205302
48. Blakemore, J.S.: Approximations for fermi-dirac integrals, especially the function $f_{1/2}(\eta)$ used to describe electron density in a semiconductor. Solid-State Electronics **25**(11), 1067–1076 (1982). https://doi.org/10.1016/0038-1101(82)90143-5
49. He, G., Ghosh, K., Singisetti, U., Ramamoorthy, H., Somphonsane, R., Bohra, G., Matsunaga, M., Higuchi, A., Aoki, N., Najmaei, S., Gong, Y., Zhang, X., Vajtai, R., Ajayan, P.M., Bird, J.P.: Conduction mechanisms in CVD-grown monolayer MoS_2 transistors: From variable-range hopping to velocity saturation. Nano Lett. **15**(8), 5052–5058 (2015). https://doi.org/10.1021/acs.nanolett.5b01159. (**PMID: 26121164**)
50. Wang, Y., Huang, S., Zhao, H., Liu, K.: First principles study on properties of monolayer MoS_2 under different strains. Brazilian J. Phys. **51**, 1230–1236 (2021). https://doi.org/10.1007/s13538-021-00927-2
51. Saha, D., Mahapatra, S.: Analytical insight into the lattice thermal conductivity and heat capacity of monolayer MoS_2. Physica E: Low-dimensional Syst. Nanostructures **83**, 455–460 (2016). https://doi.org/10.1016/j.physe.2016.01.013
52. Li, W., Carrete, J., Mingo, N.: Thermal conductivity and phonon linewidths of monolayer MoS_2 from first principles. Appl. Phys. Lett. **103**(25), 253103 (2013). https://doi.org/10.1063/1.4850995
53. Yalon, E., Aslan, B., Smithe, K.K.H., McClellan, C.J., Suryavanshi, S.V., Xiong, F., Sood, A., Neumann, C.M., Xu, X., Goodson, K.E., Heinz, T.F., Pop, E.: Temperature-dependent thermal boundary conductance of monolayer MoS_2 by Raman thermometry. ACS Appl. Mater. & Interfaces **9**(49), 43013–43020 (2017). https://doi.org/10.1021/acsami.7b11641